The effects of X-ray absorption variability in NGC 4395

E. Nardini[1*] and G. Risaliti[1,2]

[1] *Harvard-Smithsonian Center for Astrophysics, 60 Garden St., Cambridge, MA 02138, USA*
[2] *INAF - Osservatorio Astrofisico di Arcetri, L.go E. Fermi 5, 50125 Firenze, Italy*

Released Xxxx Xxxxx XX

ABSTRACT

We present a new X-ray analysis of the dwarf Seyfert galaxy NGC 4395, based on two archival *XMM-Newton* and *Suzaku* observations. This source is well known for a series of remarkable properties: one of the smallest estimated black hole masses among Active Galactic Nuclei (of the order of $\sim 10^5 M_\odot$), intense flux variability on very short time-scales (a few tens of seconds), an unusually flat X-ray continuum ($\Gamma \sim 1.4$ over the 2–10 keV energy range). NGC 4395 is also characterized by significant variations of the X-ray spectral shape, and here we show that such behaviour can be explained through the partial occultation by circumnuclear cold absorbers with column densities of $\sim 10^{22}$–10^{23} cm^{-2}. In this scenario, the primary X-ray emission is best reproduced by means of a power law with a standard $\Gamma \sim 1.8$ photon index, consistent with both the spectral slope observed at higher energies and the values typical of local AGN.

Key words: galaxies: active – galaxies: individual: NGC 4395 – X-rays: galaxies.

1 INTRODUCTION

The central regions of the dwarf spiral galaxy NGC 4395 show most of the common signatures of nuclear activity. The optical and ultraviolet (UV) spectra reveal prominent high-ionization forbidden lines on top of a nearly feature-less continuum, and broad wings corresponding to gas velocities in excess of $\sim 10^3$ km s^{-1} are detected in the permitted lines (Filippenko & Sargent 1989). Contrary to the objects of the same kind, the emission-line properties, the optical to X-ray variability pattern and the inferred accretion rate of NGC 4395 are those typical of the Seyfert class, of which this source is usually considered to represent the least luminous member. Different methods have been employed in the last years to derive the mass of its central black hole: the estimate obtained through reverberation mapping is $M_{\mathrm{BH}} \simeq 3.6 \times 10^5 M_\odot$ (Peterson et al. 2005), but the lack in this galaxy of a significant bulge and the stringent upper limit of 30 km s^{-1} on its velocity dispersion suggest an even lower value, of the order of $\sim 10^4$–$10^5 M_\odot$ (Filippenko & Ho 2003). Anyhow, the engine of NGC 4395 falls somewhere between the stellar-mass black holes found in Galactic X-ray binaries and the supermassive black holes residing inside active galactic nuclei (AGN). As such, it can provide critical information about the relationship between these two populations and the physics of accretion systems in general.

In the light of all these pieces of observational evidence, NGC 4395 is a true scaled-down version of an ordinary Seyfert galaxy, the only difference with respect to its high-luminosity counterparts being the much smaller mass of the central black hole. On the other hand, the X-ray observations of this source indicate an unusual spectral hardness at ~ 2–10 keV, and suggest a wide range of variations for the intrinsic photon index. The most extreme states ($\Gamma \sim 0.6$; Moran et al. 2005) are even difficult to interpret within the standard two-phase model (Haardt & Maraschi 1991), posing serious questions on the production mechanism of the X-ray emission itself. The presence of undetected absorption effects has been frequently invoked as a possible explanation. Indeed, the stronger flux variability characterizing systematically the soft X-ray bands can be attributed to a complex, multi-zone warm absorber, whose properties have been discussed in detail in several works (Iwasawa et al. 2000; Shih, Iwasawa & Fabian 2003; Dewangan et al. 2008). Here we review the two highest-quality observations of NGC 4395, performing in both cases an accurate time-resolved analysis mainly focused on neutral absorption, in order to test whether changes of its column density and/or covering factor play a role in the apparent X-ray spectral hardness of this source.

2 DATA REDUCTION AND ANALYSIS

The longest *XMM-Newton* monitoring of NGC 4395 started on 2003 November 30, for a total duration of ~ 113 ks. After the subtraction of high-background periods, the useful exposure declines to 91.4 ks. We also take into account the deep *Suzaku* observation, which was carried out on 2007 June 2–5 over a span of ~ 230 ks, corresponding to a net integration

* E-mail: enardini@cfa.harvard.edu

time of 101.3 ks. We have followed the standard procedures for the reduction of the event files, and extracted the source and background spectra from circular regions with radii of $30''(XMM\text{-}Newton)$ and $2'(Suzaku)$. In the first case, for the sake of clarity only EPIC-pn data are presented here and plotted in the figures, even though the MOS spectra have been checked throughout and give fully consistent results; in the second one, instead, only the data from the front-illuminated detectors of the X-ray imaging spectrometer (XIS) have been examined, after merging the XIS0 and XIS3 spectra. The spectral analysis has been performed using the XSPEC v12.6 fitting package. All the uncertainties are given at the 90 per cent confidence level ($\Delta\chi^2 = 2.71$) for the single parameter of interest.

2.1 The *XMM-Newton* observation

We first restricted our analysis to the energies above 1 keV, following the customary approach of fitting the spectrum averaged over the whole observation to obtain a benchmark model. We achieved a fully acceptable fit ($\chi^2_\nu \simeq 1.03$ for 1390 degrees of freedom, with no obvious structure in the residuals) through a simple model consisting of a power law with photon index $\Gamma \simeq 1.18$, a narrow iron emission line with equivalent width EW = $91(\pm 30)$ eV, and a partial neutral absorber whose column density and covering fraction are $N_{\rm H} \simeq 1.3 \times 10^{22}$ cm^{-2} and $f_{\rm cov} \simeq 0.6$, respectively.[1] No reflection component is strictly required for the continuum: however, by adding a PEXRAV model (Magdziarz & Zdziarski 1995) for physical consistency and forcing its strength to match the width of the narrow iron line,[2] the fit is slightly improved ($\Delta\chi^2 \simeq -8$ with the loss of one d.o.f.) and the power-law photon index steepens to $\simeq 1.24$. Both cases above yield a formally satisfactory fit, yet the flat slope of the intrinsic continuum deserves a thorough investigation. This result would actually confirm one of the most remarkable features of NGC 4395, which had been previously caught by *Chandra* even in harder states (see Moran et al. 2005). In any case, the typical value of $\Gamma \sim 1.3$–1.5 is still unusually low, compared with both the distribution of photon indices found in local AGN (e.g. Bianchi et al. 2009) and the average 15–150 keV spectrum of the source measured by the Burst Alert Telescope (BAT) onboard *Swift* ($\Gamma \simeq 2.0$; Fig. 1).

A viable explanation for such a discrepancy is the presence of a complex (variable) absorber, strongly modifying the observed spectral shape of NGC 4395 below ~ 10 keV. The extrapolation of the basic model down to 0.5 keV supports this working assumption: the apparent extra emission at 0.5–0.7 keV, in fact, hints at absorption effects in the ~ 0.7–1.5 keV range rather than at a genuine soft excess like the one detected in a large fraction of Seyfert galaxies (e.g. Boller, Brandt & Fink 1996; Porquet et al. 2004). Moreover, a clearly time-dependent behaviour of the X-ray source is revealed not only by the overall flux light curve but also by
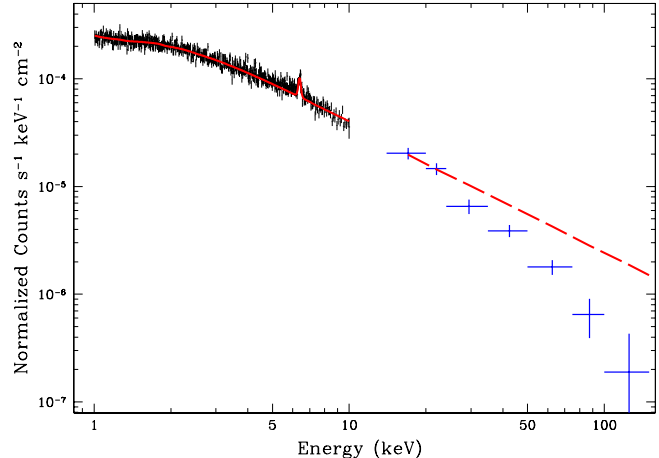
---

[1] Galactic absorption has been frozen throughout at $N_{\rm H} = 1.8 \times 10^{20}$ cm^{-2} (Kalberla et al. 2005).
[2] Assuming solar iron abundance, this implies that continuum reflection and line emission are associated with the same reprocessing component (e.g. George & Fabian 1991).

Figure 1. X-ray emission of NGC 4395 above 1 keV and best fit (red solid line) of the entire *XMM-Newton* observation. The extrapolation of this benchmark model at higher energies (red dashed line) is compared with the average spectrum extracted from the *Swift*/BAT 58-month catalog, whose shape is perfectly described by a simple power law with $\Gamma \simeq 2.0(\pm 0.2)$.
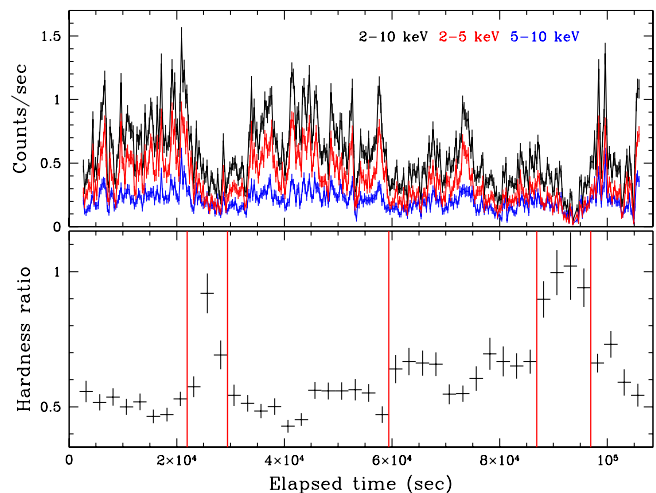

Figure 2. Top panel: 2–10 keV light curve of NGC 4395 during the *XMM-Newton* observation (in black). The behaviour of the source at 2–5 (red) and 5–10 keV (blue) is also shown separately, adopting a bin width of 250 s. Bottom panel: 5–10 over 2–5 keV hardness ratio, with the time resolution degraded by a factor of ten. The vertical red lines define the six intervals over which individual spectra have been extracted in our time-resolved analysis.

the hardness ratio (HR) evolution. It is well established that NGC 4395 is characterized by strong variations of the X-ray flux on time-scales as short as a few hundreds of seconds (Fig. 2, upper panel): the fractional rms variability amplitude during the *XMM-Newton* observation under review is exceptionally high (~ 90 per cent at 0.5–2 keV; see Vaughan et al. 2005). On top of these fluctuations of the intrinsic X-ray brightness, mainly related to the workings of the primary source, significant *spectral* variations are also evident from the visual inspection of the HR light curve (Fig. 2, lower panel). The observed HR pattern can be accounted for through either changes of the column density or, alternatively, oscillations of the continuum slope: this proves that

a time-averaged spectral analysis is not sufficient to fully understand the nature of the X-ray emission of NGC 4395. The hardness ratio is defined here as the ratio between the 5–10 keV and the 2–5 keV flux, thus it is especially sensitive to values of $N_{\rm H}$ of the order of 10^{22}–10^{23} cm^{-2}. As already mentioned, the spectral complexity and the larger fractional rms variability below $\sim$2 keV are likely due instead to a multi-zone warm absorber, whose presence has been revealed since the early *ASCA* observations of the source (Iwasawa et al. 2000; Shih et al. 2003). We anyway note that this is not a critical point, since the HR evolution is only used to select the appropriate intervals for the subsequent time-resolved spectral analysis, which is crucial to validate or dismiss the suggested interpretation.

The shape of the HR light curve reveals two periods of sudden spectral hardening around $\sim$25 and 90 ks; this hints at increased opacity, which would mainly affect the 2–5 keV band. According to Fig. 2, six different regimes of the hardness ratio can be roughly defined. In this framework, the minor HR fluctuations on very short time-scales can be due to a flickering of the photon index in response to variations of the physical conditions in the disc/corona system, but the statistics is not enough for a complete investigation of these aspects. Regardless of this, our aim is to check whether a reasonable configuration of the neutral absorber allows us to recover a steeper intrinsic photon index for the X-ray emission of NGC 4395.

In order to obtain an adequate description of the entire 0.5–10 keV spectral range, we included in the reference model above also an APEC component for the soft thermal emission (Smith et al. 2001) and a two-zone warm absorber, whose complex effects have been already pointed out in several previous works (see also Dewangan et al. 2008). In our analysis we have assumed that the soft emission, warm absorption and reflection features do not vary in the course of a $\sim$100 ks long observation: since the light crossing time over a distance of a gravitational radius ($r_{\rm g} = GM_{\rm BH}/c^2$) is of the order of one second, the reflection component is expected to change significantly in response to the primary continuum only if the scattering material is located well within $\sim 10^5 r_{\rm g}$ from the centre (as in the disc reflection scenarios; e.g. Nardini et al. 2011). Similarly, the soft emission likely arises from a very extended region, while the warm absorber, in principle, could lie much closer to the X-ray source (but see Blustin et al. 2005): if this is the case, we are just sampling its average properties.[3] On the other hand, Γ, $N_{\rm H}$ and $f_{\rm cov}$ were initially left free to evolve among the different intervals. In spite of the possible degeneracies, it turns out that the photon index and the column density are subject to very limited variations: in particular, $\Delta\Gamma < 0.2$. This suggests that Γ and $N_{\rm H}$ can be roughly treated as constant parameters as well, hence their values have been tied in all the six spectra: only the covering fraction of the cold absorber is allowed to vary with time.

On sheer statistical grounds, this model already gives a very good fit (χ^2_ν/d.o.f. = 0.994/1788, with $\Gamma \simeq 1.90$ and

---

[3] The warm absorbers have been modelled with ABSORI, adopting the nominal XSPEC values (with solar abundances) and a full covering. We are not interested in a more detailed study of this component here, hence its nature is not explored further.
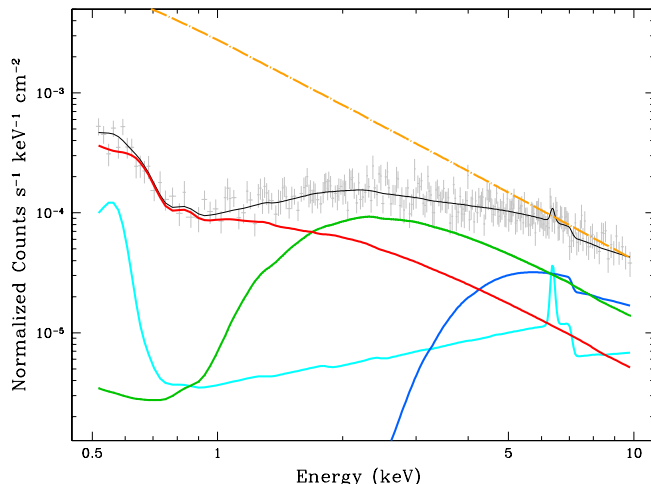
Figure 3. Illustration of the different model components for the *XMM-Newton* spectrum extracted from interval 6 (shaded in the background along with its best fit). The soft emission plus reflection features (cyan curve) are assumed to be constant over the entire observation; the spectral variations are therefore due to the relative weight of the three fractions of the intrinsic power law (dot-dashed orange line), transmitted through the warm absorber only and an additional neutral column $N_{\rm H}(1)$ or $N_{\rm H}(2)$, and plotted respectively in red, green and blue.

$N_{\rm H} \sim 2.1 \times 10^{22}$ cm^{-2}), proving that, in first approximation, $f_{\rm cov}$ alone would be able to account for all the observed spectral variability: its qualitative trend across the six intervals, in fact, fairly correlates with the shape of the HR light curve. There are some problems with the reflection efficiency, though. It is not obvious how to assess the latter quantity in the time-resolved analysis, anyway by comparing the PEXRAV amplitude to the highest flux level of the power-law continuum we obtain a reflection strength of $R \sim 7.5$, which is completely inconsistent with the moderate equivalent width of the companion iron line (George & Fabian 1991). Moreover, when extrapolated at higher energies, such component would give rise to a very flat spectrum with a prominent Compton hump at $\sim$30 keV, which is not detected by *Swift*/BAT. Given that the time-scales are extremely different, it is still possible that the source is caught in a state of large reflection during the *XMM-Newton* observation, but in this case the fluorescent iron line should be much stronger as well. Forcing R to have a standard value delivers a poor spectral description, and no improvement is achieved through the self-consistent REFLIONX table models (Ross & Fabian 2005).

As a consequence, we attempted to introduce a second partial covering cold absorber, assuming again that Γ and $N_{\rm H}(1,2)$ are constant, and $f_{\rm cov}(1,2)$ variable. The best fit quality is significantly improved (χ^2_ν/d.o.f. = 0.961/1781), while the photon index $\Gamma \simeq 1.86$ is still in excellent agreement with the average high-energy slope of the source. The presence of an additional absorber with column density of $\sim 10^{23}$ cm^{-2} removes all the previous limitations, reducing substantially the required strength of the reflection continuum (now $R \sim 1.2$). This is also clear from Fig. 3, where the different model components are disentangled to display their relative contribution in a single time segment. The ba-
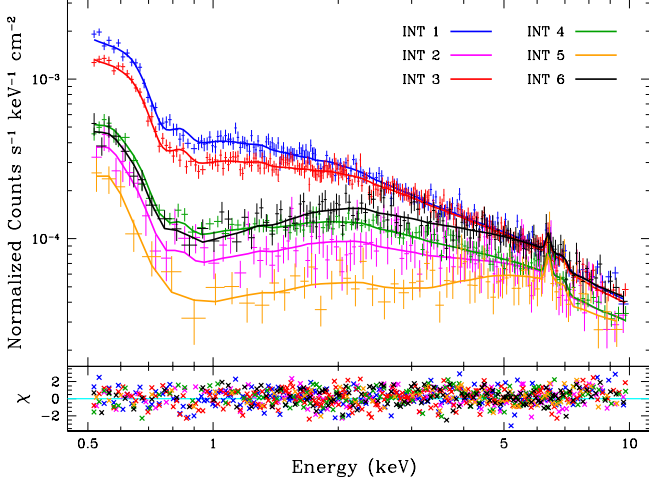
Figure 4. Top panel: spectra and best-fitting models for the six *XMM-Newton* intervals. Bottom panel: residuals in units of σ. The data are rebinned for plotting purposes only.

Table 1. Main parameters of the *XMM-Newton* and *Suzaku* best-fitting models, common to all the intervals on which our time-resolved spectral analysis has been performed. Γ: photon index; kT: temperature of the soft emission in eV; N_W, ξ_W: column density in cm^{-2} and ionization parameter in erg cm s^{-1} of the warm absorption components; EW$_{\rm Fe}$: time-averaged equivalent width of the 6.4-keV iron line in eV; R: strength of the reflected continuum; $N_{\rm H}$: column density of the neutral absorbers in cm^{-2}; $F_{\rm obs}$, $F_{\rm int}$: average observed and intrinsic 0.5–10 keV flux in erg cm^{-2} s^{-1}.

Obs.	*XMM-Newton*	*Suzaku*
Γ	1.86 ± 0.06	$1.74^{+0.12}_{-0.14}$
kT	41^{+6}_{-11}	41^*
$N_W(1)$	$0.67^{+0.03}_{-0.04} \times 10^{22}$	$0.51^{+0.18}_{-0.17} \times 10^{22}$
$\xi_W(1)$	$3.5^{+0.9}_{-0.4}$	$5.9^{+8.8}_{-3.0}$
$N_W(2)$	$1.90^{+0.45}_{-0.35} \times 10^{22}$	$1.90^* \times 10^{22}$
$\xi_W(2)$	368^{+113}_{-83}	368^*
EW$_{\rm Fe}$	64^{+35}_{-32}	81 ± 53
R	1.2 ± 1.1	$1.4^{+2.9}_{-1.3}$
$N_{\rm H}(1)$	$1.68^{+0.23}_{-0.28} \times 10^{22}$	$1.07^{+0.40}_{-0.32} \times 10^{22}$
$N_{\rm H}(2)$	$2.55^{+0.51}_{-0.46} \times 10^{23}$	$0.92^{+0.85}_{-0.42} \times 10^{23}$
$F_{\rm obs}$	6.25×10^{-12}	5.54×10^{-12}
$F_{\rm int}$	1.36×10^{-11}	9.15×10^{-12}
χ^2_ν	$1711/1781$	$1095/1146$

*: frozen value.

sic parameters of this final model are listed in Table 1, while the six individual spectra are shown in Fig. 4.

2.2 The *Suzaku* observation

In spite of the promising indications, the cold absorption scenario needs to be tested on different X-ray observations of NGC 4395 to be definitely regarded as reliable for this source. Indeed, a complex configuration consisting of both a partially and a fully covering neutral absorber (plus three warm components) has been shown to provide an adequate fit of the time-averaged spectrum reviewed here, and has been also applied with success to the short *XMM-Newton* snapshots of NGC 4395 (Dewangan et al. 2008). In general, however, the number of counts collected during the archival

observations is not sufficient to derive solid and independent constraints on our model. We have therefore analysed the only other long, high-quality monitoring of NGC 4395 that is available to date, obtained by *Suzaku* and fully discussed by Iwasawa, Tanaka & Gallo (2010). In the latter work, the time-averaged spectrum is described by means of a power-law continuum with $\Gamma \sim 1.4$, modified by a warm absorber with ionization parameter $\xi_W \sim 35$ erg cm s^{-1} and column density $N_W \simeq 2 \times 10^{22}$ cm^{-2}; a narrow iron line and neutral absorption in moderate excess of the Galactic amount are also involved. By dividing the whole observation into six segments of equal length, and allowing Γ, ξ_W and N_W to vary in turn among the six spectra, the authors suggest that a change of the photon index might account for most of the spectral variability of the X-ray source. None the less, the 15–35 keV *Suzaku*/PIN spectrum reveals a slope of $\sim 2.2(\pm 0.5)$, consistent with the *Swift*/BAT measure and possibly indicative of some undetected absorption component at lower energies.

On the wake of this conjecture, we have also performed a time-resolved analysis, yet choosing the time intervals on the grounds of the HR light curve, as usual. The 5–10 over 2–5 keV hardness ratio follows a trend which is qualitatively very similar to that shown in Fig. 2 (see e.g. the X-ray colour HR3 in Iwasawa et al. 2010): again, six different periods have been identified. We have adopted the same model defined above. However, the soft thermal emission and the high-ionization component of the warm absorber cannot be firmly constrained, hence their properties have been frozen to the values obtained in the *XMM-Newton* study. In spite of this assumption we are able to recover an excellent fit to the data, with $\chi^2_\nu/\text{d.o.f.} = 0.956/1146$. The photon index of the primary continuum is slightly flatter ($\Gamma \sim 1.75$), but its uncertainty combined with that on $N_{\rm H}(2)$ is rather large due to the lower data quality (see Fig. 5). Indeed, if Γ is bound to the *XMM-Newton* best-fitting measure the variation in terms of statistical goodness is very limited, being $\Delta\chi^2 \simeq +3$. According to an F-test, the probability of chance improvement when Γ is included among the free parameters amounts to ~ 8.3 per cent. In any case, the estimated photon index is again well above the value obtained by describing the time-averaged spectrum with a simpler model. Our results are summarized in Tables 1 and 2, and the six *Suzaku* spectra are shown in Fig. 6.

3 DISCUSSION

The cold absorption model provides a good interpretation of the spectral variability of the X-ray source during both the *XMM-Newton* and *Suzaku* observations. Moreover, considering the entries of Table 1, the basic physical quantities appear to be in fair agreement. This is a strong confirmation of the validity of the scenario explored in this work, where the changes are driven by the evolution of the covering fractions. The $f_{\rm cov}(1)$ and $f_{\rm cov}(2)$ progression is listed in Table 2. Due to the smaller uncertainties, we focus our discussion on the *XMM-Newton* case. We first point out that our model is defined in such a way that mutually exclusive regions of the X-ray source are affected by the two cold absorbers: in other words, we only consider a single-layer configuration of the neutral gas along the line of sight. All the $f_{\rm cov}$ sequences
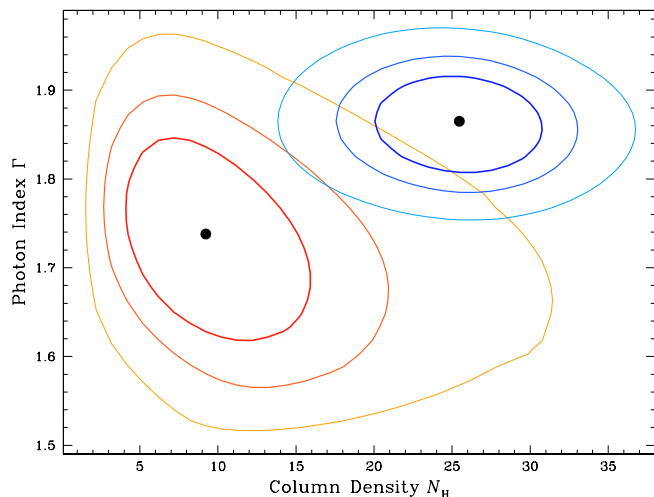
Figure 5. Confidence contours at the 68, 90 and 99 per cent level in the Γ–$N_H(2)$ space for both the *XMM-Newton* and the *Suzaku* observation. The photon index is well constrained and the two measures are in good agreement. (N_H is in units of 10^{22} cm^{-2}).
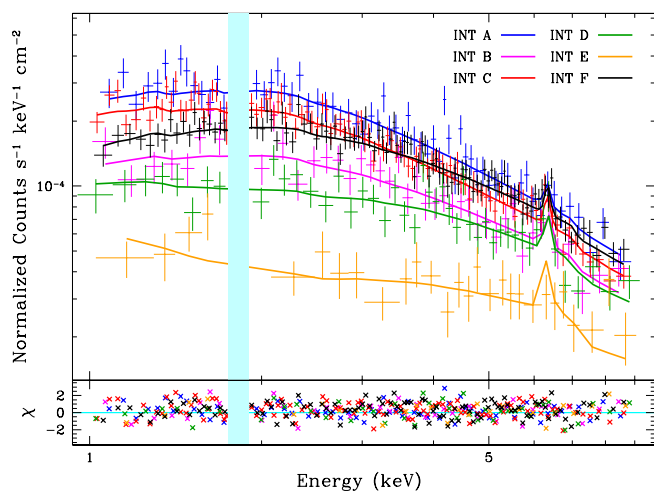

Figure 6. Same as Fig. 4 for the *Suzaku* observation. Only the 1–9 kev range is plotted for clarity, while the 1.75–1.9 keV region is excluded from the fits due to calibration uncertainties around the instrumental silicon absorption edge.

should be taken with some caution, though. The low ionization stage in one of the warm absorption component impairs to some extent the determination of $f_{cov}(1)$, while possible changes in the reflection strength on that of $f_{cov}(2)$. However, even from the face values obtained under our assumptions, some interesting considerations can be drawn. It is now $f_{cov}(2,t) = \{0.38, 0.60, 0.31, 0.47, 0.79, 0.53\}$ that shows a tighter correlation with the HR light curve: the peaks during periods 2 and 5 might be explained in terms of *eclipses* from individual *clouds* (e.g. Lamer, Uttley & McHardy 2003; Risaliti et al. 2007). Given that the duration of such events is ~10 ks, a typical dimension of the X-ray source of ~$10^2 r_g$ corresponds to a transverse velocity of the putative clouds of ~10^3 km s^{-1}, placing the obscuring gas at the broad-line region scale. The size and the shape of these blobs are not precisely known. Yet, our time-resolved analysis suggests that different column densities are present along the line of

Table 2. Time evolution of the covering fractions during the two observations and χ_ν^2 decomposition over the single intervals. By definition, $f_{cov}(0)$ is the fraction of the X-ray source subject to warm absorption only.

INT	$f_{cov}(0)$	$f_{cov}(1)$	$f_{cov}(2)$	χ_ν^2
1	0.62±0.11	< 0.03	0.38±0.11	440/424
2	0.14±0.05	0.26±0.09	0.60±0.12	118/106
3	0.49±0.10	0.20±0.06	0.31±0.12	488/473
4	0.22±0.06	0.31±0.09	0.47±0.13	395/428
5	0.07±0.04	0.14±0.07	0.79±0.09	55/55
6	0.13±0.03	0.34±0.08	0.53±0.10	215/235
A	0.36±0.19	0.64±0.20	< 0.16	117/128
B	0.28±0.18	0.48±0.23	0.24±0.20	92/81
C	0.40±0.17	0.60±0.18	< 0.11	375/393
D	0.26±0.17	0.24±0.20	0.50±0.22	76/91
E	0.38±0.23	< 0.25	0.62±0.25	40/27
F	0.22±0.12	0.50±0.15	0.28±0.13	405/388

sight at the same time. The range of variations in f_{cov} implies that the number of intervening clouds is very limited (a few at most, see Fig 7), and that their size is comparable to the dimensions of the X-ray source. The extreme case entails a single irregular and inhomogeneous absorber.

The physical situation is then expected to be rather complex. In this view, the X-ray absorbers that we have included should be only regarded as a linear combination of the *real* ones, whose exact geometrical structure cannot be probed with the present data quality. The large disparity (roughly an order of magnitude) between the column densities involved, and specifically the fact that $N_H(1) < \sigma_{N_H}(2)$, hints at a multi-layer configuration of the cold absorber, where the two phases have a different location and are superimposed in part on one another when seen in projection. Such a scheme can be envisaged as in Fig. 8: only the broad-line region component, with $N_H \sim 10^{23}$ cm^{-2}, has a time-dependent covering fraction ($f_{cov} \sim$ 0.3–0.8). Conversely, the absorption system with lower column density is constant (or at least variable over much longer scales), and can be associated with a more distant gaseous component, within a narrow-line or torus-like region. Indeed, this would be consistent with both the optical classification of NGC 4395 as a type 1.5–1.8 Seyfert galaxy (Ho et al. 1997; Panessa et al. 2006) and the large covering factor of the emission-line regions with respect to the central source (Kraemer et al. 1999). The broad- and narrow-line regions are expected to be responsible for some of the UV to X-ray absorption detected in NGC 4395 (Crenshaw et al. 2004), and evidence for the identification of the rapidly variable X-ray absorber with the broad-line emitting clouds have been recently found in other Seyfert galaxies (e.g. Maiolino et al. 2010; Risaliti et al. 2011). In this perspective, the frequency and amplitude of the variations in N_H and/or f_{cov} would be linked to the degree of clumpiness of the circumnuclear environment at the different scales.

Once the *Suzaku* data are taken into account, all the considerations made above still hold, even though the uncertainties on the key parameters are quite large, and the smaller difference between $N_H(1)$ and $N_H(2)$ makes the covering fraction patterns less meaningful. Apart from the speculations on the physical and geometrical structure of the cold ab-
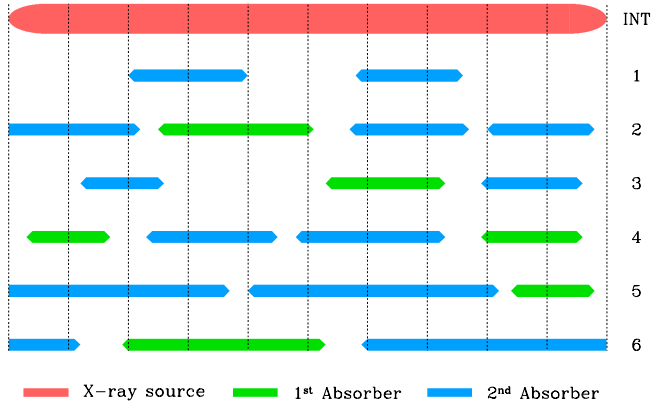
Figure 7. Sketch of the simplest structure of the X-ray cold absorber, consisting of individual clouds at the same distance from the X-ray source but with different column densities. The covering factors across the six *XMM-Newton* intervals have been chosen to reproduce the values listed in Table 2. The number of clouds simultaneously crossing the line of sight and their size are limited by the rapid changes of f_{cov}. Even a single blob with irregular shape and non-uniform physical properties is consistent with the observed variability pattern. (The observer is located towards the bottom of the page).

Figure 8. Same as Fig. 7, but an alternative configuration is assumed: the absorption component with lower column density has a constant covering fraction of 0.35 and is external to the system of clouds responsible of the X-ray spectral variability (see the discussion in the text).

sorption system, the scenario outlined in this work has the other great advantage of strengthening the correlation between NGC 4395 and the high-luminosity AGN population. First, it gives reasons for the X-ray spectral hardness of this source, reconciling the estimate of its photon index with the typical values found among AGN; secondly, neutral absorption variability systematically occurs in a significant fraction of active galaxies, the prototypical case being another type 1.8 Seyfert, NGC 1365 (e.g. Risaliti et al. 2009). Our findings then represent a further point of contact between NGC 4395 and its more massive and luminous counterparts. Incidentally, it is also worth noting that the intrinsic 0.5–10 keV emission of NGC 4395 implied in this cold absorption scheme is larger than the observed one by just a factor of $\sim$2 (Table 1). Taking advantage of the *Swift*/BAT spectral constraints, the resulting 0.5–100 keV luminosity is $\sim$6–8 $\times 10^{40}$ erg s^{-1}, which exceeds the usual estimates of the bolometric luminosity (see also Moran et al. 2005; Iwasawa et al. 2010). Depending of the exact value of the black hole mass, the Eddington ratio of NGC 4395 could be much closer to $\sim$0.01 than previously thought.

4   CONCLUSIONS

We have discussed a possible interpretation of the X-ray spectral hardness usually observed in the low-luminosity active galaxy NGC 4395. This source harbours in its centre a black hole with estimated mass of $\sim$10$^5 M_\odot$, and it is one of the few known objects whose study can shed light on the links between the physics of accretion processes in Galactic black hole binaries and AGN. In spite of being a genuine Seyfert galaxy in many respects, NGC 4395 remains a somewhat puzzling source because of the inferred flatness of its primary X-ray continuum. The existence of complex absorption effects has often been proposed as a likely explanation. Here we have provided for the first time an example
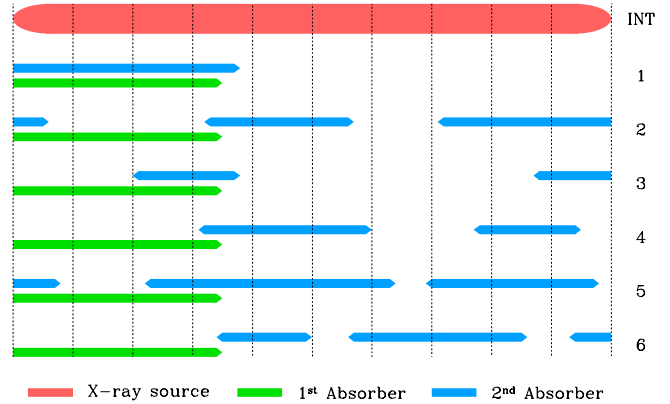
of these effects based on observational evidence, by reviewing the two highest-quality looks of NGC 4395 taken by *XMM-Newton* and *Suzaku*: in both cases, a time-resolved analysis shows that the spectral evolution of the source can be interpreted by means of a two-phase neutral absorber with variable covering factor. As a first approximation, this cold absorber is identified with the system of broad-line clouds, allowing for a double-peaked N_H distribution. The low column density component can otherwise be attributed to an external narrow-line or torus-like region, with nearly constant f_{cov}. This is presumably an oversimplification of the physical and geometrical structure of the circumnuclear environment (which is known to comprise also a complex, multi-zone warm absorber), but even the existence of a single partial-covering cold screen cannot be completely ruled out on statistical grounds.

We stress that the absorption variability scenario presented here is not unique, and different models based on intrinsically flat X-ray continua (with significant changes of either the photon index or the reflection strength) can describe the observed behaviour of this source equally well. This interpretation, however, fits into the analogy between the properties of NGC 4395 and those of *standard* high-luminosity Seyfert galaxies, many of which are systematically affected by X-ray absorption variability due to the clumpiness of their circumnuclear regions. Moreover, it allows us to retrieve in a natural way a $\Gamma \simeq 1.8$ photon index below 10 keV, in perfect agreement with the *Swift*/BAT spectral slope and the usual values measured among AGN. No alternative explanation would then be required for the intrinsic 2–10 keV flatness of NGC 4395.

REFERENCES

Bianchi S., Guainazzi M., Matt G., Fonseca Bonilla N., Ponti G., 2009, A&A, 495, 421

Blustin A. J., Page M. J., Fuerst S. V., Branduardi-Raymont G., Ashton C. E., 2005, A&A, 431, 111

Boller T., Brandt W. N., Fink H., 1996, A&A, 305, 53

Crenshaw D. M., Kraemer S. B., Gabel J. R., Schmitt H. R., Filippenko A. V., Ho L. C., Shields J. C., Turner T. J., 2004, ApJ, 612, 152

Dewangan G. C., Mathur S., Griffiths R. E., Rao A. R., 2008, ApJ, 689, 762

Filippenko A. V., Sargent W. L. W., 1989, ApJ, 342, L11

Filippenko A. V., Ho L. C., 2003, ApJ, 588, L13

George I. M., Fabian A. C., 1991, MNRAS, 249, 352

Haardt F., Maraschi L., 1991, ApJ, 380, L51

Ho L. C., Filippenko A. V., Sargent W. L. W., Peng C. Y., 1997, ApJS, 112, 391

Iwasawa K., Tanaka Y., Gallo L. C., 2010, A&A, 514, A58

Kalberla P. M. W., Burton W. B., Hartmann D., Arnal E. M., Bajaja E., Morras R., Pöppel W. G. L., 2005, A&A, 440, 775

Kraemer S. B., Ho L. C., Crenshaw D. M., Shields J. C., Filippenko A. V., 1999, ApJ, 520, 564

Lamer G., Uttley P., McHardy I. M., 2003, MNRAS, 342, L41

Magdziarz P., Zdziarski A. A., 1995, MNRAS, 273, 837

Maiolino R., et al., 2010, A&A, 517, A47

Moran E. C., Eracleous M., Leighly K. M., Chartas G., Filippenko A. V., Ho L. C., Blanco P. R., 2005, AJ, 129, 2108

Nardini E., Fabian A. C., Reis R. C., Walton D. J., 2011, MNRAS, 410, 1251

Panessa F., Bassani L., Cappi M., Dadina M., Barcons X., Carrera F. J., Ho L. C., Iwasawa K., 2006, A&A, 455, 173

Peterson B. M., et al., 2005, ApJ, 632, 799

Porquet D., Reeves J. N., O'Brien P., Brinkmann W., 2004, A&A, 422, 85

Risaliti G., Elvis M., Fabbiano G., Baldi A., Zezas A., Salvati M., 2007, ApJ, 659, L111

Risaliti G., et al., 2009, MNRAS, 393, L1

Risaliti G., Nardini E., Salvati M., Elvis M., Fabbiano G., Maiolino R., Pietrini P., Torricelli-Ciamponi G., 2011, MNRAS, 410, 1027

Ross R. R., Fabian A. C., 2005, MNRAS, 358, 211

Shih D. C., Iwasawa K., Fabian A. C., 2003, MNRAS, 341, 973

Smith R. K., Brickhouse N. S., Liedahl D. A., Raymond J. C., 2001, ApJ, 556, L91

Vaughan S., Iwasawa K., Fabian A. C., Hayashida K., 2005, MNRAS, 356, 524